ELSEVIER

Cement & Concrete Composites 25 (2003) 145–152

Cement & Concrete Composites

www.elsevier.com/locate/cemconcomp

Application of X-ray computed tomography to characterise the early hydration of calcium aluminate cement

T.J. Chotard [a,*], M.P. Boncoeur-Martel [b,*], A. Smith [a,*], J.P. Dupuy [b], C. Gault [a]

[a] *Groupe d'Etude des Matériaux Hétérogènes (GEMH, EA 3178), Ecole Nationale de Céramique Industrielle, 47 à 73 Avenue Albert Thomas, 87065 Limoges Cedex, France*

[b] *Département de Radiologie, Centre Hospitalier Universitaire DUPUYTREN, 2, avenue Martin Luther King, 87042 Limoges Cedex, France*

Received 2 October 2001; accepted 29 October 2001

Abstract

Techniques that monitor in situ the setting and hardening of calcium aluminate cements (CACs) are of interest to the engineering community. This paper focuses on one non-destructive technique, X-ray computed tomography (CT). The early hydration of the cement can be followed from a few minutes to a few hours after mixing. This technique is based on both X-ray absorption measurements and qualitative observations in chosen axial cross-sections. Results concerning an aluminous cement, Secar 71, are presented (water-to-cement weight ratio: 0.33; duration: 0–24 h). Information deduced from these measurements clearly show that a strong variation of X-ray absorption values occurs during the early age of hydration. Both quantitative and qualitative analyses of CT data allow a chronology of cement setting to be proposed.

Keywords: Hydration; Calcium aluminate cement; Computed tomography

1. Introduction

Calcium aluminate cements (CACs) are a range of ceramic materials which are of interest not only to industrialists since they cover a wide market in civil engineering, refractory industry or specific niches, but also to the materials science community [1–3]. In particular, the complete understanding of hydration mechanisms at an early age, from a few minutes to a few hours after mixing the constituents, is not totally achieved. Several approaches to describe the nature and the formation of hydrates during this early stage have been reported in the literature [4–29]. Conductivity and pH measurements, usually carried out on dilute systems, enable to describe hydration as a dissolution and precipitation process [4,5]. Classical techniques such as thermal analysis, X-ray diffraction (XRD), scanning electron microscopy (SEM) give information about the chemical nature and the morphology of the hydrates. Besides these characterisations which have been done ex situ, i.e. after stopping cement hydration, there are in situ analyses by proton and aluminium nuclear magnetic resonance [10,11] or neutron diffraction [12,13] which have been carried out on small volumes of specimen. There is a need for characterisation techniques which are capable of providing information on larger samples and in situ. In this respect, ultrasonic characterisations can fulfil this dimensional requirement [16–28] and provides a non-destructive evaluation of the mechanical characteristics of the material. This last aspect is essential to optimise the drying process and the mechanical performance of the final object. An example of practical interest is to be able to improve the production yield of pre-cast elements for the refractory industry. Amongst other parameters, the mechanical performance is related to the cement density and its variation as a function of setting time. One classical method to determine bulk density changes is based on Le Chatelier's shrinkage. However, this procedure gives only an average behaviour. In the present paper, we wish to introduce another in situ and

* Corresponding authors.

E-mail addresses: t.chotard@ensci.fr (T.J. Chotard), boncoeur@unilim.fr (M.P. Boncoeur-Martel), a.smith@ensci.fr (A. Smith).

0958-9465/03/$ - see front matter
PII: S0958-9465(01)00063-4

non-destructive technique to characterise the cement hydration at early age. It is based on X-ray computed tomography (CT), which has already proven to be reliable for the evaluation of density and porosity distributions on green and sintered compacts [30–34]. CT is appropriate for the inspection of a range of components being non-contact, non-invasive and unlimited by the complexity of internal and external surfaces. Moreover, high-energy CT systems can penetrate large objects fabricated from a wide variety of materials. The results reported here refer to Secar 71.

2. Experimental procedure

2.1. Preparation of the cement paste

Although it is well known that CACs are nowadays used in very small amounts in refractory castables, we have chosen to use a large sample of cement paste alone in order to focus specifically on the hydration reaction of the paste. The reason behind this choice is that CAC has its own reactivity and mixing it with other constituents, such as sand or an admixture, can modify the hydration mechanism due to possible chemical interactions between the cement and these other products.

One batch of paste has been prepared with a water-to-cement weight ratio (W/C) equal to 0.33 which is commonly used in industry. This batch, called SE033, has been mixed according to the normalised procedure No. CEN 196-3. After mixing, the paste was poured into a silicone foam mould (90 mm × 90 mm × 30 mm) prior to CT measurements. Dimensions of the mould have been chosen to be representative of volume effects. Silicone foam has been selected for the moulds in order to follow the shrinkage of the cement paste during hydration. A possible separation between the mould and the tested material is then avoided. The experiments were carried out at 20 °C and 95% relative humidity. The cement used was Secar 71 from Lafarge Aluminate. Its composition and physical characteristics (supplied by Lafarge) are given in Table 1.

2.2. Characterisation techniques

2.2.1. Description of CT technique

X-ray computed tomography was used to monitor density changes in the material during hydration from a few minutes to a few hours after mixing. This technique allows the transmittance, T, through the length d of the sample under test to be measured. T is defined by Beer–Lambert's law:

$$T = \frac{I}{I_0} = \mathrm{e}^{-(\mu d)}, \tag{1}$$

where I and I_0 are the final and the initial intensities, respectively. μ corresponds to the linear absorption coefficient (in cm^{-1}); it depends on the wavelength of the radiation, the nature of the absorber and is directly related to the atomic density of the material [30].

Eq. (1) only applies to monochromatic X-rays and to a perfectly homogeneous material. A typical system for medical or industrial applications uses a source which emits polychromatic electromagnetic waves. Additionally, the tested material in the present case, i.e. cement paste, is far from being homogeneous. The CT system used is assumed to operate on volume elements which are small enough to be considered homogeneous. As the absorption (also called attenuation = 1− transmittance), can be easily deduced from Eq. (1), the collection of absorption measurements over many views allows a 2D cross sectional image (CT image) to be mathematically constructed. The values of the absorption coefficients are transformed into CT numbers using the international Hounsfield scale:

$$\text{CT number} = \frac{\mu_{\text{material}} - \mu_{\text{water}}}{\mu_{\text{water}}} \times 1000 \text{ (HU)}, \tag{2}$$

where μ_{material} and μ_{water} are the linear absorption coefficients (in cm^{-1}) of the material under test and water, respectively. The CT numbers, in Hounsfield units (HU), are representatives of the mean X-ray absorption associated which each element area of the CT image. The result of this computer treatment is a map of linear absorption coefficients within the studied cross-section. Table 2 gives the CT scan parameters of the equipment (model high Speed Advantage from GE).

Table 1
Chemical composition, either in nature of cementitous phase or in oxide, for the cement

Chemical composition		Percentage (wt%)
Cementitous phase	$CaAl_2O_4$ (or CA)	56
	$CaAl_4O_7$ (or CA_2)	38
	$Al_2O_3\alpha$	<6
	$Ca_{12}Al_{14}O_{33}$ (or $C_{12}A_7$)	<1
Oxide	CaO	26.6–29.2 wt%
	Al_2O_3	69.8–72.2 wt%

Table 2
CT scan standard parameters

Parameter	Standard setting
Field of view (FOV)	150 mm
Slice thickness	1 mm/5 mm
Type of slice	Contiguous
Slice per sample	90/20
Display matrix	512×512 pixels
Reconstruction matrix	512×512 pixels
Spatial resolution	$(150/512) \approx 300$ μm
Exposure time	1 s
X-ray tube voltage	120 kV
X-ray tube current	200 mA

In order to describe the absorption variations as a function of setting time on either a bulk or local scale, 2D reconstruction of the sample was determined from slices 1 mm thick. These slices were contiguous. Considering the initial dimensions of the sample, 90 views were taken in order to scan the whole specimen. For three selected slices (two towards the sample edges, one in the middle), different types of CT measurements were carried out; the scanning configuration is shown in Fig. 1.

On each slice, the variations of CT number along longitudinal (y) and vertical (z) lines were taken (Line Graph). In addition, the average values of CT number for special regions of interest (ROI) of the slice were also taken. Finally, a histogram of the CT images (CT numbers distribution) was recorded. Fig. 2 illustrates these different measurements.

2.2.2. Background on CACs hydration process

The full description of hydration mechanism of calcium aluminate cements requires the use of several techniques such as calorimetry, conductivity, X-ray diffraction, thermal analysis and scanning electron microscopy.

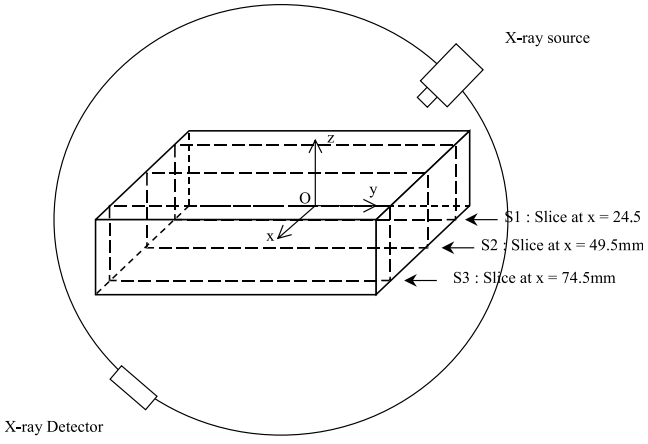

Fig. 1. Scanning configuration of the cement specimen.

The most encountered theory based on the results obtained involves congruent dissolution of anhydrous phases followed by precipitation of hydrates (Le Chatelier's theory). Experiments on dilute systems have been interpreted from this theory. According to this approach, grains of CA dissolve under the form of Ca^{2+} and $Al(OH)_4^-$ ions. Their concentration rapidly reaches supersaturation compared with that is necessary for hydrate formation. Therefore, nuclei of hydrates start to form. After this nucleation phase, also called the "dormant period", a growth step takes place. It is characterised by a massive precipitation of hydrates which is accompanied with a significant heat generation. During this stage, crystallised hydrates are developing. In reality, though these hydrates form very early, i.e. just after mixing the constituents, they cannot be detected immediately by XRD [27]. Two hypotheses about this last remark can be done. The germs of formed hydrates (in their crystal form) are too small to be detected by XRD or more probably the germs are in their amorphous form. It is well known that the type of formed hydrates in CACs is temperature dependent. Four different types of hydrates can be present in the material, namely CAH_{10}, C_2AH_8, C_3AH_6 and AH_3 in cement notation (C for CaO, A for Al_2O_3 and H for H_2O), according to the following reactions:

$$CA + 10H \rightarrow CAH_{10} \quad T < 15\ ^\circ C \tag{3}$$

$$2CA + 11H \rightarrow C_2AH_8 + AH_3 \quad 15\ ^\circ C < T < 30\ ^\circ C \tag{4}$$

$$3CA + 12H \rightarrow C_3AH_6 + 2AH_3 \quad T > 30\ ^\circ C \tag{5}$$

The mentioned temperature limits are not strict. In the present experiment, since the dimension of the sample is fairly large, an important self-heating has been observed (highest temperature measured inside the sample: 64 °C). Consequently, depending on the position inside the cement sample, reactions (3), (4) or (5) can occur.

3. Results and discussion

3.1. Qualitative observations

Fig. 3 shows the CT images obtained for slice S2 and for increasing times after mixing. A notable evolution of the greyscale can be observed as long as the curing time increases.

From 0 h to approximately 3 h after mixing, the corresponding CT image (Fig. 3(a)) exhibits a fairly homogeneous level of greyscale which suggests that the X-ray absorption of the tested medium is also relatively homogeneous. A more accurate examination of the micrograph shows that a clearer layer can be observed at the bottom of the sample. This specific zone, which

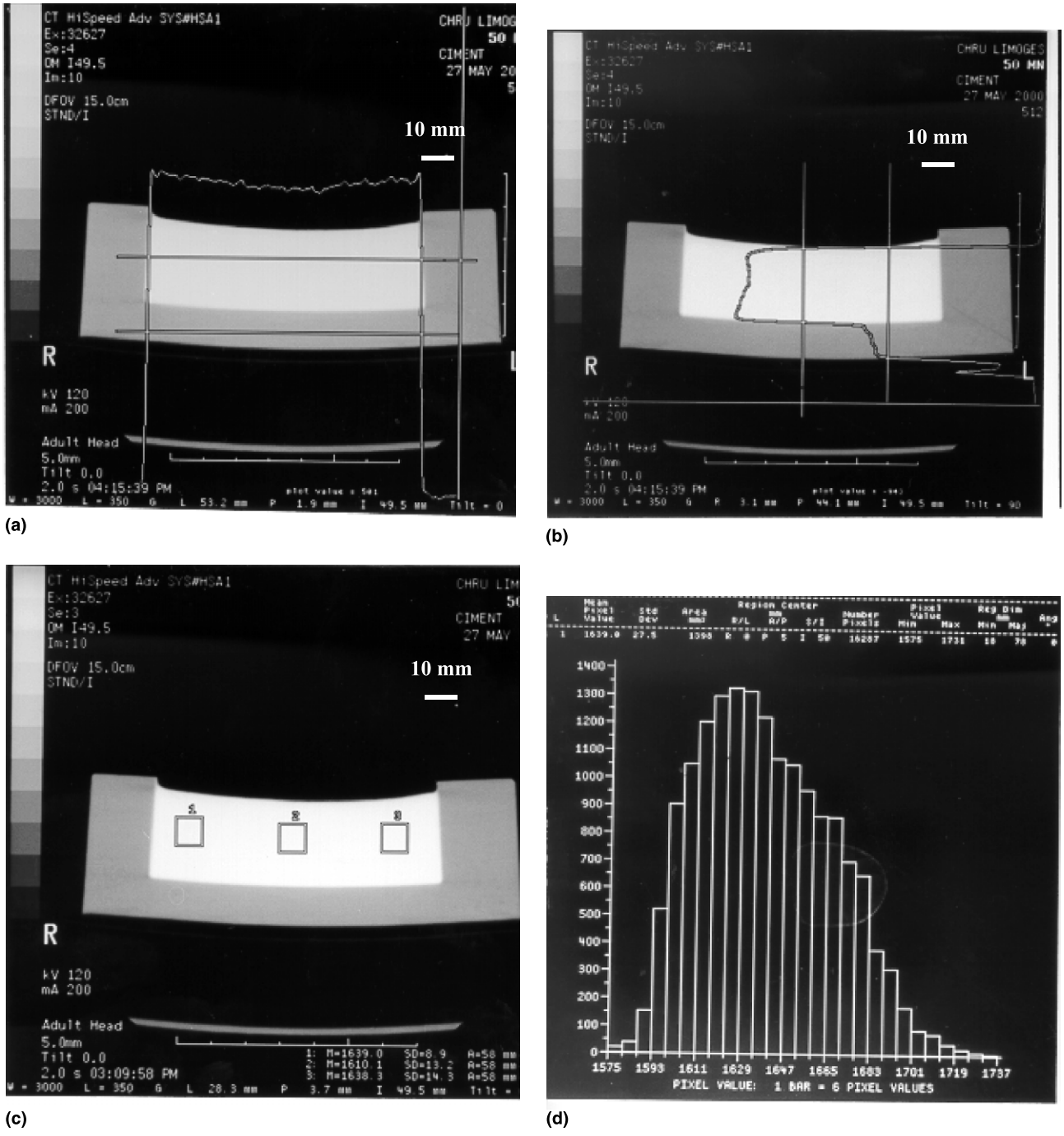

(a) (b) (c) (d)

Fig. 2. Examples of typical CT measurements: (a) longitudinal line graph, (b) vertical line graph, (c) ROI (1: left, 2: centre, 3: right), (d) histogram.

corresponds to a localised high-density area, can be probably related to an early sedimentation phenomenon due to the difference of density between the water and the anhydrous powder. As already said, during this period, called the dormant period, a small number of hydrates starts to nucleate. This stage has already been characterised [35,36] by electrical measurements at high frequency (1 MHz–1.8 GHz). These hydrates, which are probably amorphous, are of nanometric dimensions; this is too small to be resolved by the CT scan. Therefore, the CT image relates to the simultaneous presence of water and cement.

At 3.5 h after mixing (Fig. 3(b)), a dark area appears in the centre of the specimen. This reveals a notable drop in the X-ray absorption of the material. It is important to note that the highest temperature value re-

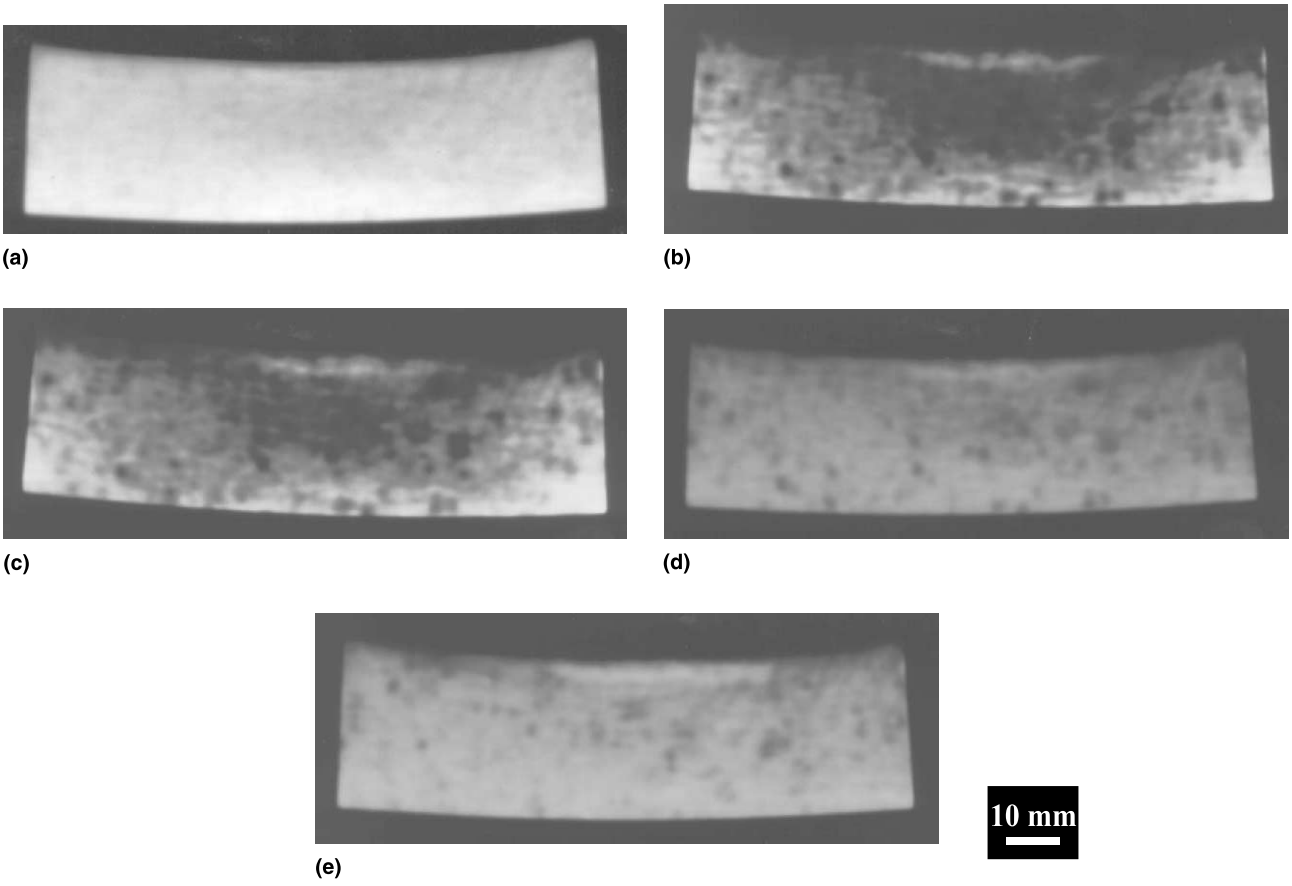

Fig. 3. CT images for the S2 slice and for different times after mixing: (a) 1 h, (b) 3.5 h, (c) 5 h, (d) 5.75 h, (e) 24 h.

corded inside the sample is around 64 °C. At this temperature, some water can evaporate. The combination of this water evaporation and the chemical reaction taking place in the sample could induce a notable variation of the average X-ray absorption coefficient. Moreover, some rounded patterns are clearly visible in the CT image. This observation could be related to a well known phenomenon in CAC pastes, the ''nodular setting'', where precipitation occurs in only a few isolated nuclei, forming nodules [37]. Besides, an absorption gradient is observed between the centre and the edges of the specimen under test. This fact can be related to the heterogeneity of the thermal field which exists in the material during setting. The massive formation of hydrates is associated with an exothermic reaction [5,10,28]. In our case, the diffusion of heat in the material is heterogeneous and can induce a gradient in hydrate formation within the volume of the sample. In the heart of the sample, where the temperature is the highest, the hydration is more advanced than at the edges. As the curing time increases, the hydration continues and a clearing of the corresponding CT image (Fig. 3(c)) is observed. To summarise, from 3 to 5.75 h after mixing, where massive hydration takes place, the X-ray absorption decreases (Fig. 3(b)), and subsequently increases (Figs. 3(c) and (d)). During this period, the material is also stiffening [28].

Beyond this time, the evolution of the greyscale on the CT image is less marked as the setting time increases (comparison between Fig. 3(d) and (e)), and the grey seems to be more uniform. The greyscale of the corresponding CT image (Fig. 3(e)) is slightly darker than the initial one (Fig. 3(a)). This observation denotes that the final average X-ray absorption of the set cement is lower than in the initial mix.

4. Quantitative measurements

In order to validate the preceding hypothesis, some quantitative measurements have been performed on several slices at different curing times. The histograms of the corresponding CT images, already discussed in the previous paragraph, are presented in Fig. 4.

This graph clearly shows what we can call a ''boomerang effect'' of the average X-ray absorption variation. The initial value is nearby 1650 HU. After 2 h, a drop from 1650 HU to approximately 1300 HU is

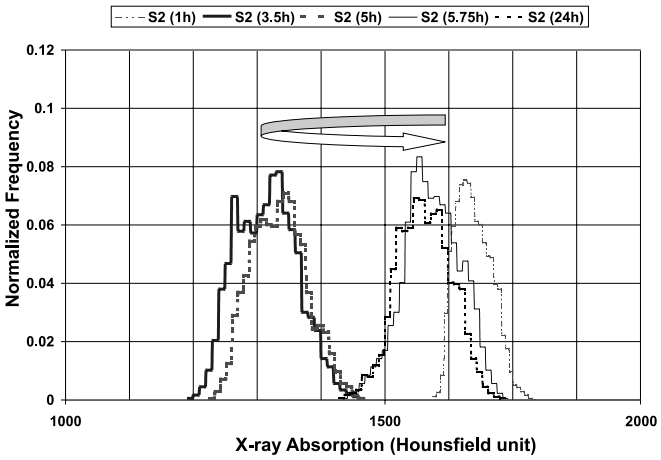

Fig. 4. Histograms of the S2 slice deduced from Fig. 6.

observed. From 5 h, the average X-ray absorption increases again to reach its final value (1550 HU). Considering this variation of X-ray absorption, some explanation can be proposed. As we know, the X-ray absorption coefficient depends on the wavelength of the radiation, the nature of the absorber and is directly related to the atomic density of the material. The organisation of the atoms in the considered volume can also induce a variation of this coefficient. It has been shown recently [28] that during the dormant period, the hydrates which start to nucleate are probably in an amorphous form and as the reaction continues, a massive precipitation of these amorphous germs occurs. Thereafter, a crystallised form of the hydrates can be detected by XRD measurement [27]. It is important to note that the original mix contains crystalline particles (the anhydrous powder). It is the same for the final product (anhydrous and hydrates). A possible explanation of the "boomerang" variation of the average X-ray absorption coefficient could be summarised as follows: crystalline particles in the initial mix (anhydrous powder) keep the average absorption coefficient at around its initial value. Then, the massive precipitation of small amorphous germs induces a local variation of the atomic density especially in the centre of the sample where the highest temperature has been recorded. At this time, water evaporates. This variation can notably affect the average X-ray absorption of the sample. Afterwards, hydrates start to crystallise; this crystallisation can be responsible for a local variation of the atomic density which affect the value of the absorption coefficient.

Fig. 5 presents the results of X-ray absorption measurements in specific regions of interest (ROI) for the CT images. This graph emphasises the existence of an X-ray absorption gradient between the centre and the edges of the sample during the hydration process. This

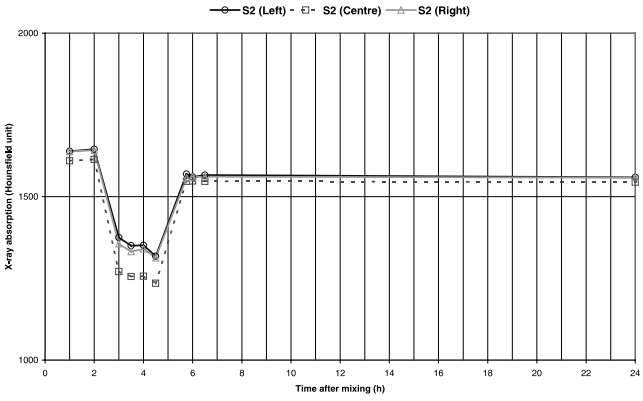

Fig. 5. Density measurements as a function of setting time for the S2 slice at different ROI.

measurement confirms the observations made on CT images (Fig. 3). It is important to note that the observed gradients involve the overall volume of the sample, which is confirmed by line graph measurements (Fig. 6).

If we compare the evolution of the different sets of data, namely qualitative observations, CT measurements such as histograms, ROI and line graphs, we can propose the following chronology, divided into five principal stages which are pointed out in Fig. 7:

Stage 1 (0–2 h after mixing): The X-ray absorption distribution is relatively homogeneous in the sample. During this initial period, hydrates are probably formed only in very low amounts.

Stage 2 (2–3 h after mixing): A strong decrease in the X-ray absorption value of the specimen is observed. It can be explained by massive production of hydrates in amorphous form and also by evaporation of water.

Stage 3 (3–4.5 h after mixing): Slight evolution of X-ray absorption while the hydration continues.

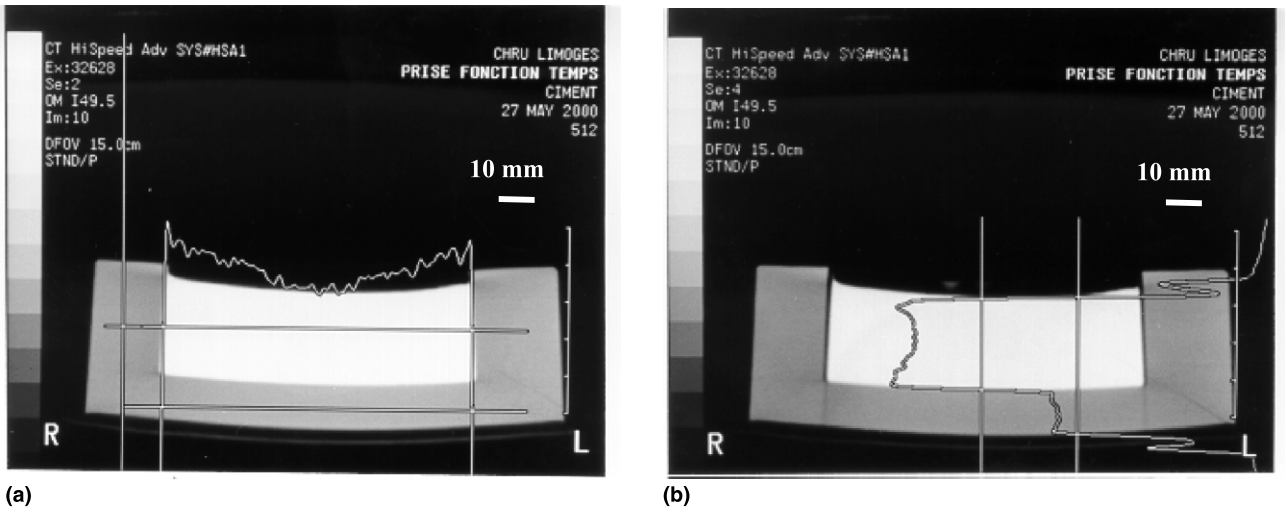

Fig. 6. Line graph measurements for S2 slice at 3.5 h after mixing : (a) along a longitudinal axis, (b) along a vertical axis.

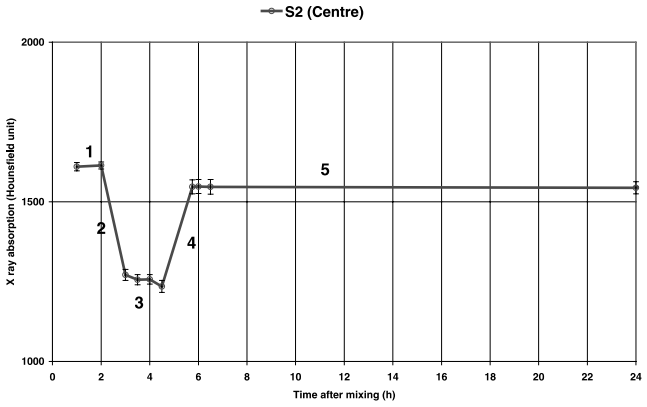

Fig. 7. Density measurement as a function of setting time for the S2 slice and at the centre.

Stage 4 (4.5–5.75 h after mixing): Increase of the X-ray absorption of the sample is closely related to the crystallisation of hydrates. Beginning of the stiffening of the specimen (setting).

Stage 5 (5.75–24 h after mixing): The sample reaches its final hardened state.

5. Conclusion

This paper describes the analysis of CT images and CT measurements performed on Secar 71 cement paste just after mixing (W/C = 0.33). Qualitative observations and quantitative measurements enable us to propose some conclusions:

- CT can be beneficial to describe the X-ray absorption variations in relation to the progression of the hydration process in the cement paste.
- CT gives important information concerning the X-ray absorption gradients which take place in the specimen. The heterogeneous character of the setting process is clearly emphasised. Hydration probably starts in the heart of the sample before spreading all over. In addition, a "boomerang effect" of the X-rays absorption values is pointed out.

This technique provides another non-destructive in situ tool, which can be applied to fairly large specimens (cement, mortars or concrete). It allows us to propose a qualitative description of the chronology of hydration. A complete interpretation of hydration phenomena needs the combination of this technique with other in situ measurements (XRD, DTA, and TG) and ex situ techniques (ultrasonic velocity, acoustic emission monitoring).

References

[1] Scrivener KL, Cabiron JL, Letourneux R. High-performance concretes from calcium aluminate cements. Cem Concr Res 1999;29:1215–23.
[2] Midgley HG. In: Mangabhai RJ, editor. Calcium aluminate cements. London: Chapman & Hall; 1990. p. 1–13.
[3] Jiang SP, Mutin JC, Nonat A. Studies on mechanism and physico-chemical parameters at the origin of the cement setting. I. The fundamental processes involved during the cement setting. Cem Concr Res 1995;25:779–89.
[4] Capmas A, Menetrier-Sorrentino D, Damidot D. Effect of temperature on setting times of calcium aluminate cements. In: Mangabhai RJ, editor. Calcium aluminate cements. London: Chapman & Hall; 1990. p. 65–80.
[5] Sharp JH, Bushnell-Watson SM, Payne DR. The effect of admixtures on the hydration of refractory calcium aluminate cements. In: Mangabhai RJ, editor. Calcium aluminate cements. London: Chapman & Hall; 1990. p. 127–41.

[6] Scrivener KL, Taylor HFW. Microstructural development in pastes of calcium aluminate cement. In: Mangabhai RJ, editor. Calcium aluminate cements. London: Chapman & Hall; 1990. p. 41–51.
[7] Cottin B. Etude au microscope électronique de pâtes de ciment alumineux hydratées en C_2AH_8 et CAH_{10}. Cem Concr Res 1971; 2:177–86.
[8] Chatterjiand S, Majumdar AJ. Studies of the early stages of paste hydration of high alumina cements. I: Hydration of individual aluminate. Ind Concr J 1966:51–5.
[9] Richard N. Structure et propriétés élastiques des phases cimentières de mono-aluminate de calcium. PhD Thesis, Paris VI University, France, 1996.
[10] Greenslade DJ, Williamson DJ. The use of Nuclear Magnetic Resonance (NMR) in the study of high alumina cement hydration. In: Mangabhai RJ, editor. Calcium aluminate cements. London: Chapman & Hall; 1990. p. 81–95.
[11] Rashid S, Turrillas X. Hydration kinetics of $CaAl_2O_4$ using synchrotron energy-dispersive diffraction. Thermochim Acta 1997; 302:25–34.
[12] Barnes P, Clark SM, Hausermann D, Henderson E, Fentiman CH, Muhamad MN, Rashid S. Time-resolved studies of the early hydration of cements using synchrotron energy-dispersive diffraction. Phase Trans 1992;39:117–28.
[13] Monteiro PJM, King MS. Experimental studies of elastic wave propagation in high-strength mortar. Am Ceram Soc Test Mater 1998:68–74.
[14] Harker AH, Schofield P, Stimpson BP, Taylor RG, Temple JAG. Ultrasonic propagation in slurries. Ultrasonics 1991;29:427–38.
[15] Cutard T, Fargeot D, Gault C, Huger M. Time delay and phase shift measurement for ultrasonic pulses using autocorrelation methods. J Appl Phys 1994;75:1909–13.
[16] Öztürk T, Rapoport J, Popovics JS, Shah SP. Monitoring the setting and hardening of cement-based materials with ultrasound. Concr Sci Eng 1999;1:83–91.
[17] Sayers CM, Grenfell RL. Ultrasonic propagation through hydrating cement. Ultrasonics 1993;31:147–53.
[18] Sayers CM, Dahlin A. Propagation of ultrasound through hydrating cement pastes at early times. Adv Cem Bas Mater 1993;1:12–21.
[19] Cannard G, Orcel G, Prost J. Le suivi de la prise des ciments par ultrasons. Bull Liaison Lab Phys Chim 1990;168:89–95.
[20] Keating JD, Hannant J, Hibbert AP. Correlation between cube strength, ultrasonic pulse velocity and volume change for oil well cement slurries. Cem Concr Res 1989;19:715–26.
[21] Keating JD, Hannant J, Hibbert AP. Comparison of shear modulus and pulse velocity techniques to measure the build-up of structure in fresh cement pastes used in oil well cementing. Cem Concr Res 1989;19:554–66.
[22] Belkheiri L, Bocquet M, Abidi ML, Zoukaghe M. Continuous ultrasonic measurements during setting and hardening of building materials. Mater Struct 1999;32:59–62.
[23] Labouret S, Looten-Baquet I, Bruneel C, Frohly J. Ultrasound method for monitoring rheology properties evolution of cement. Ultrasonics 1998;36:205–8.
[24] Popovics S, Popovics JS. Ultrasonic testing to determine water-cement ratio for freshly mixed concrete. Cem Concr Aggr 1998;20(2):262–8.
[25] Stepisnik J, Lukac M. Measurement of cement hydration by ultrasonics. Ceram Bull 1981;60:481–3.
[26] Boumiz A, Vernet C, Cohen-Tenoudji F. Mechanical properties of cement pastes and mortars at early ages. Adv Cem Bas Mater 1996;3:94–106.
[27] Chotard TJ, Gimet-Bréart N, Smith A, Fargeot D, Bonnet JP, Gault C. Application of ultrasonic testing to describe the hydration of calcium aluminate cement at the early age. Cem Concr Res 2001;3:405–12.
[28] Richardson IG. The nature of the hydration products in hardened cement pastes. Cem Concr Comp 2000;22:97–113.
[29] Glisic B, Simon N. Monitoring of concrete at very early age using SOFO sensor. Cem Concr Comp 2000;22:115–9.
[30] Phillips DH, Lannutti JJ. Measuring physical density with X-ray computed tomography. NDT Int 1997;30:339–50.
[31] Deis TA, Lannutti JJ. X-ray computed tomography for evaluation of density gradient formation during the compaction of spray-dried granules. J Am Ceram Soc 1998;81:1237–47.
[32] Phillips DH, Lannutti JJ. X-ray computed tomography for the testing and evaluation of ceramic processes. Am Ceram Soc Bull 1992;71:1410–6.
[33] Lu P, Lannutti JJ. X-ray computed tomography and mercury porosimetry for evaluation of density evolution and porosity distribution. J Am Ceram Soc 2000;83:518–22.
[34] Kong CM, Lannutti JJ. Localized densification during compaction of alumina granules: the stage I–II transition. J Am Ceram Soc 2000;83:685–90.
[35] Smith A, Bonnet JP, Abelard P, Blanchart P. Electrical characterisation of aluminous cement at the early age in the 10 Hz–1 GHz frequency range. Cem Concr Res 2000;30:1057–62.
[36] Chotard TJ, Gimet-Bréart N, Smith A, El Hafiane Y, Bonnet JP, Abelard P, et al. Electrical characterisation at high frequency (1 MHz–1 GHz) of an aluminous cement. An Chim Sci Mater 2000;25:S197.
[37] Lamour VRH, Monteiro PJM, Scrivener KL, Fryda H. Microscopic studies of the early hydration of calcium aluminate cements. In: Mangabhai RJ, Glasser FP, editors. Calcium aluminate cements. London: IOM Communications; 2001. p. 169–80.